



PEM fuel cell applications of doped (Ni, Zr) metal alloyed Pt/C cathode catalysts

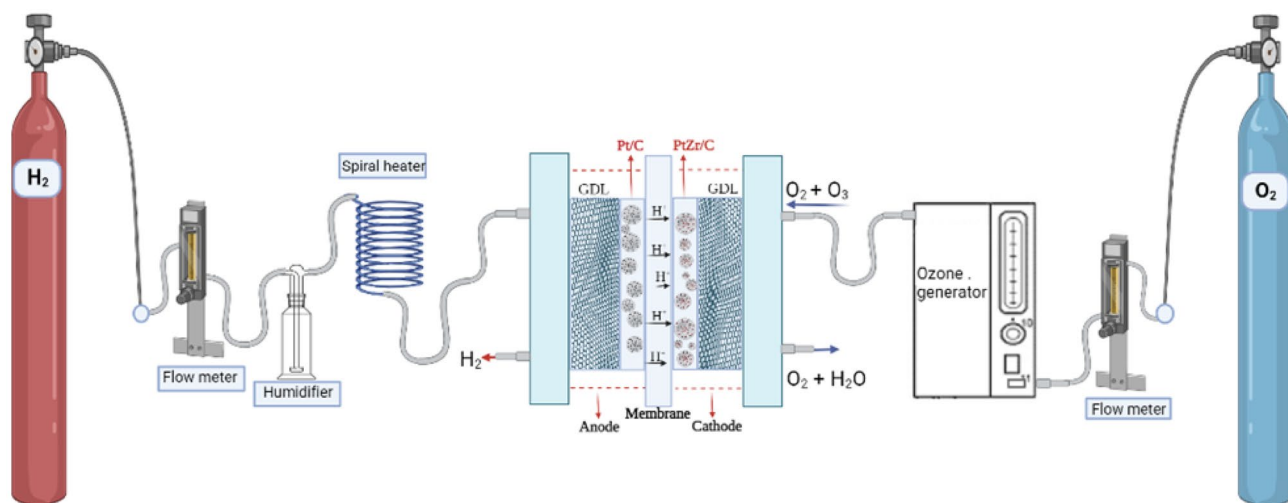
Abdurrahman Akdag¹ · Sabit Horoz² · Ömer Şahin³ · Arzu Ekinci⁴

Received: 30 March 2024 / Accepted: 29 June 2024
© The Author(s), under exclusive licence to Springer Nature B.V. 2024

Abstract

This investigation reported the performance of PEMFC cathode electrocatalysts produced from platinum, zirconium, and nickel alloys with varying atomic ratios. XRD, SEM, and EDX analyses were performed to investigate the structural and morphological properties of the synthesized catalysts. The studies evaluated electrochemical properties, specifically the ORR and the ECSA activity. Based on XRD data, the average crystallite diameters of Pt/C, PtZr₂/C, and PtZr₂Ni/C catalysts were calculated to be 4.95 nm, 4.33 nm, and 3.35 nm, respectively. Pt/C, PtZr₂/C, and PtZr₂Ni/C catalysts were used as cathode electrocatalysts in a single cell, and polarization curves were generated for each catalyst at temperatures of 40 °C, 50 °C, 60 °C, and 70 °C, respectively. It was determined that the PtZr₂Ni/C and PtZr₂/C catalysts had better performance than the Pt/C catalyst. Ozone, a powerful oxidizing agent, is another strategy for enhancing the cathodic process. The activity of PtZr₂Ni/C catalyst used as cathode electrocatalyst increased with increasing cell temperature in both H₂/O₂ and H₂/O₃ usage, and the power density values at 70 °C cell temperature were calculated as 165.87 mWcm⁻² and 242.08 mWcm⁻², respectively.

Graphical Abstract



Keywords Electrocatalyst · PEMFCs · PtZr/C catalyst · PtZrNi/C catalyst · Ozone

1 Introduction

Proton exchange membrane fuel cells (PEMFCs) are a promising technology, operating at low temperatures with high power efficiency and producing environmentally friendly, effective

Extended author information available on the last page of the article

energy and sustainable devices in the energy industry [1–3]. The membrane electrode assembly (MEA) is the heart of a PEM fuel cell since the oxidation and reduction of half-cell processes and proton conduction occurs [4–7]. The preparation of anode and cathode electrodes for MEAs involves a variety of techniques, including impregnation reduction, spread and spraying, catalytic powder deposition, catalytic decaling, painting, electro-deposition, and sputter deposition [8]. Among the existing methods, the impregnation reduction technique is prevalent. The impregnation technique is the most widely used for the deposition of platinum nanoparticles on the surface of carbonaceous supporting materials. Impregnation method has been widely employed to prepare platinum-based catalyst materials as a simple and cost-effective process [9]. The usage of platinum (Pt) metal and the slow kinetics of the oxygen reduction reaction (ORR) on the cathode side contribute to the prohibitively high cost of PEMFCs, which is the primary factor limiting their widespread use [10–14]. Thus, various Pt–M alloys, such as Pt–Cr, Pt–Co, Pt–Fe, Pt–Ni, Pt–Mo, Pt–Cu, and Pt–Pd [14–27], have been extensively studied to develop the ORR kinetics and stability in the electrodes. The addition of an appropriate second metal to Pt to produce a Pt alloy (PtM) catalyst affects the geometric and electronic properties of the Pt metal, which affects the ORR activity and stability of the Pt/C catalyst [28–30]. ZrO₂ is desirable for catalyst support because it is an amphoteric oxide with acid and basic sites. Because it is an amphoteric oxide, which means it has both basic and acidic sites, it may be easier for carbon oxides and steam to stick to its surface, which lowers its coke resistance [31–34]. One way to improve the cathodic reaction's performance is to use a powerful oxidizing agent. It is considered that ozone (O₃) is one of the most powerful oxidizing agents that are currently accessible [35–39]. Researchers have also treated fuel cell parts like the carbon support and electrolyte membrane with ozone [35, 40]. This study compares the ORR activity and stability of the zirconium and nickel metal-doped Pt alloy catalyst, which has never been done before as far as we know. This study focuses on using zirconium metal, which reduces the amount of Pt, is very resistant to temperature and corrosion, and shows superconducting properties at low temperatures. In this study, the ORR activity and stability of the synthesized catalysts were compared for the first time by doping both Ni and Zr metals separately into the Pt/C catalyst using oxygen and ozone as the cathode gases to reduce the Pt loading and increase the catalytic activity of the catalyst.

2 Experimental

2.1 Chemicals

Sodium borohydride (NaBH₄, 99%), ethanol (96%), isopropyl alcohol (99.9%), formic acid (85%), and Nafion solution

(5% dispersion) were purchased from Sigma Aldrich; Platinum(II) chloride (PtCl₂), Nickel(II) nitrate hexahydrate, and zirconium(IV) chloride (ZrCl₄) are purchased from Alfa Aesar. Sulfuric acid is purchased from Merck.

2.2 Synthesis of nanocatalyst

Pt:Ni:Zr (1:2:1 molar ratio) and PtZr_x ($x = 1, 2, \text{ and } 3$) catalysts based on carbon were synthesized using the chemical reduction technique. The reducing agents employed in this study were sodium borohydride and formic acid, while the metal precursors utilized were platinum chloride, zirconium chloride, and nickel nitrate. A metal loading to support 20 wt% was made to generate all catalysts. First, an appropriate quantity of PtCl₂ and a metal precursor like ZrCl₄ were dissolved in water to create the PtZr/C, PtZr₂/C, and PtZr₃/C catalysts. The details of the experimental study are included in our previous work in which we synthesized Pt/C [41].

2.3 PEM fuel cell testing

The active area of the MEAs used in these PEMFC single-cell tests was 1.0 × 1.0 cm². The anode layer used the Pt/C catalyst, whereas the cathode layer used the Pt/C, PtZr_x/C, and PtZr₂Ni/C catalysts, respectively. The details of the experimental work are included in our previous work [41]. Ozone is a gas, but it is highly unstable, thus in order to deliver and measure the quantity of ozone that is present at the fuel cell input, an ozone generator and a detector were used [42–44]. In the H₂/O₃ PEMFCs experiment, ozone gas that was created by an ozone generator is shown in Fig. 1 as a schematic representation of how it was used [35].

2.4 Characterization of the catalysts

To investigate the morphological and structural characteristics of Pt/C, PtZr₂/C, and PtZr₂Ni/C catalysts were characterized by using scanning electron microscopy (SEM), Energy dispersive X-ray spectroscopy (EDX), and X-ray diffraction (XRD). The morphological and structural properties of catalysts were determined by XRD (Rigaku X-ray diffractometer with Cu K α radiation ($\lambda = 154.059$ pm), Japan) and SEM (ZEISS-EVO 50 instrument, Carl Zeiss NTS GmbH, Germany) measurements, respectively. The basic element components of catalysts were determined by EDX (Bruker, Quantax ED-XS, Germany) analysis.

2.5 Electrochemical measurements of catalysts

Various electrochemical measurement techniques, such as electrochemical impedance spectroscopy (EIS), cyclic voltammetry (CV), chronoamperometry, and chronopotentiometry are employed for the purpose of conducting

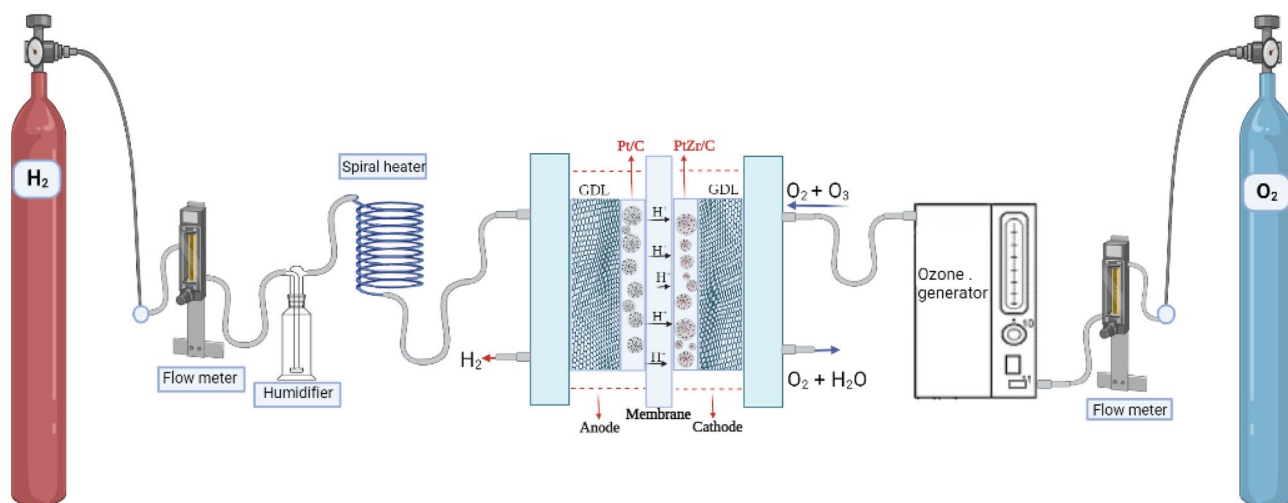


Fig. 1 The experimental the design for H_2/O_3 PEMFCs

electrochemical analyses. The 0.5 M H_2SO_4 solution is used for the measurements. Electrochemical testing is done using the CHI 660E apparatus. The working electrode was a glassy carbon electrode with a diameter of 3 mm, the reference electrode was $Ag/AgCl$ (3 M, KCl), and the counter electrode was a platinum (Pt) plate. The cyclic voltammetry (CV) measurements were conducted using a scan rate of 50 mVs^{-1} . The chronoamperometry measurements were conducted at a potential of 0.4 V. The chronopotentiometry measurements in this experiment are conducted using a current of $2\text{ }\mu\text{A}$. Impedance measurements for alternating current are acquired by establishing a voltage level of 0.5 V and subjecting the signal to a consistent amplitude of 7 mV across a frequency span ranging from 10^5 to 10^2 Hz. Before CV measurements, the solution was saturated with N_2 gas. The solution was saturated with O_2 gas before chronoamperometry, chronopotentiometry and impedance measurements. For 30 min, 5 mg of catalyst was sonicated in a solution containing 40 μl of nafion (5 wt%) and 960 μl of ethanol.

3 Results and discussion

3.1 Characterization

XRD diffraction patterns of synthesized Pt/C, $PtZr_2/C$, and $PtZr_2Ni/C$ catalysts are indicated in Fig. 2. The diffraction peak observed at an angle of $2\theta = 24.71^\circ$ corresponds to the crystallographic plane denoted as (002) in the hexagonal lattice of Vulcan XC-72 carbon.

The diffraction peaks of (111), (200), (220), and (311) planes are seen, which correspond to the face-centered cubic (FCC) crystalline structure of Pt at $2\theta(0) = 39.74, 46.33, 67.25, \text{ and } 81.60$, in that order [45]. The $PtZr_2/C$ catalyst,

on the other hand, exhibits planes at $2\theta = 39.91, 46.07, 67.41, \text{ and } 81.56$ for planes (111), (200), (220), and (311), respectively. It also exhibits $2\theta = 39.625, 45.98, 67.31, \text{ and } 81.64$ planes for (111), (200), (220), and (311) planes in the $PtZr_2Ni/C$ catalyst, respectively [45]. The $PtZr_2/C$ catalyst, on the other hand, exhibits planes at $2\theta = 39.91, 46.07, 67.41, \text{ and } 81.56$ for planes (111), (200), (220), and (311), respectively. It also exhibits $2\theta = 39.625, 45.98, 67.31, \text{ and } 81.64$ planes for (111), (200), (220), and (311) planes in the $PtZr_2Ni/C$ catalyst, respectively [46, 47].

The $PtZr_2/C$ catalyst had a slight positive shift at the 2θ position at the characteristic peaks. The $PtZr_2Ni/C$ catalyst, on the other hand, had a slight negative shift and a slight decrease in the intensity of the peaks compared to the Pt/C catalyst. This

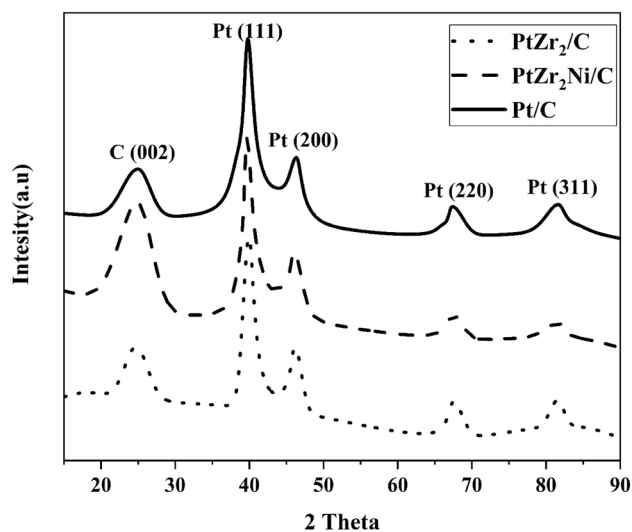


Fig. 2 XRD analyzes of electrocatalysts

implies a contraction of the lattice and the formation of an alloy [48, 49]. In the XRD results, there are no peaks corresponding to Ni metal and its oxides. Therefore, the structure of the alloy catalyst PtNi is also fcc [50]. The absence of obvious peaks of Zr or its crystalline oxide could be due to either the Zr atoms combining with the Pt atoms to form an alloy or their presence as amorphous Zr atoms [51]. The Scherrer equation [47] was employed to determine the average size of crystallites in Pt/C, PtZr₂/C, and PtZr₂Ni/C catalysts, utilizing the crystal plane of Pt (111) [52].

$$d = 0,9\lambda/(\beta\cos\theta) \quad (1)$$

The average size of a catalyst's crystallite is calculated to be 4.95 nm for Pt/C, 4.33 nm for PtZr₂/C, and 3.35 nm for PtZr₂Ni/C. The presence of Zr-doped particles reduced the crystallite size of the Pt (111) peak. Figure 3 reveals the changes in the Pt/C, PtZr₂/C, and PtZr₂Ni/C surface morphologies. As can be observed, the Pt alloy is distributed randomly throughout both surface regions.

Figure 3a shows the clumping of Pt/C on the surface. In addition, the inclusion of Zr metal appears to result in the formation of minute voids and distributed agglomerates on the catalyst's surface (Fig. 3b). Surface fractures were less noticeable, and agglomerations resembling cotton formed when Ni metal was added (Fig. 3c). The presence of cracks could potentially lead to an increased effective surface area. Catalysts typically exhibit a microstructure characterized by carbon particles with a voluminous and fluffy composition, similar to cotton, embedded with Pt alloy catalyst nanoparticles. Elemental mapping and EDX analysis confirm the equidistant distribution of Pt, Zr, and Ni on the catalyst surface (Fig. 4).

Typical Zr signals at 2.2 keV, Ni signals at 0.9 keV, and Pt signals at 2.4 keV were also seen in the EDX spectra of platinum, nickel, and zirconium metals in Fig. 4. EDX analyses also showed that these bimetallic samples were free from impurities such as chlorine. The EDX spectra in Fig. 4 show that Pt is present in Pt/C and coexists with Ni in PtZr₂Ni/C [53]. EDX spectra were used to make estimates of the weight percent of Pt/C, PtZr₂/C, and PtZr₂Ni/C catalysts; the results are described in Table 1

The Zr metal is not visible in the EDX spectrum. This may be a result of the overlap between the energy peaks of Pt and Zr. The presence of Zr metal on the surface likely contributed to an increase in the catalyst activity by making the surface more porous.

3.2 Electrochemical properties of nanocatalysts

3.2.1 Cyclic voltammetry measurement

Figure 5 displays the cyclic voltammograms of nanocatalysts composed of Pt/C, PtZr₂/C, and PtZr₂Ni/C. Peaks in

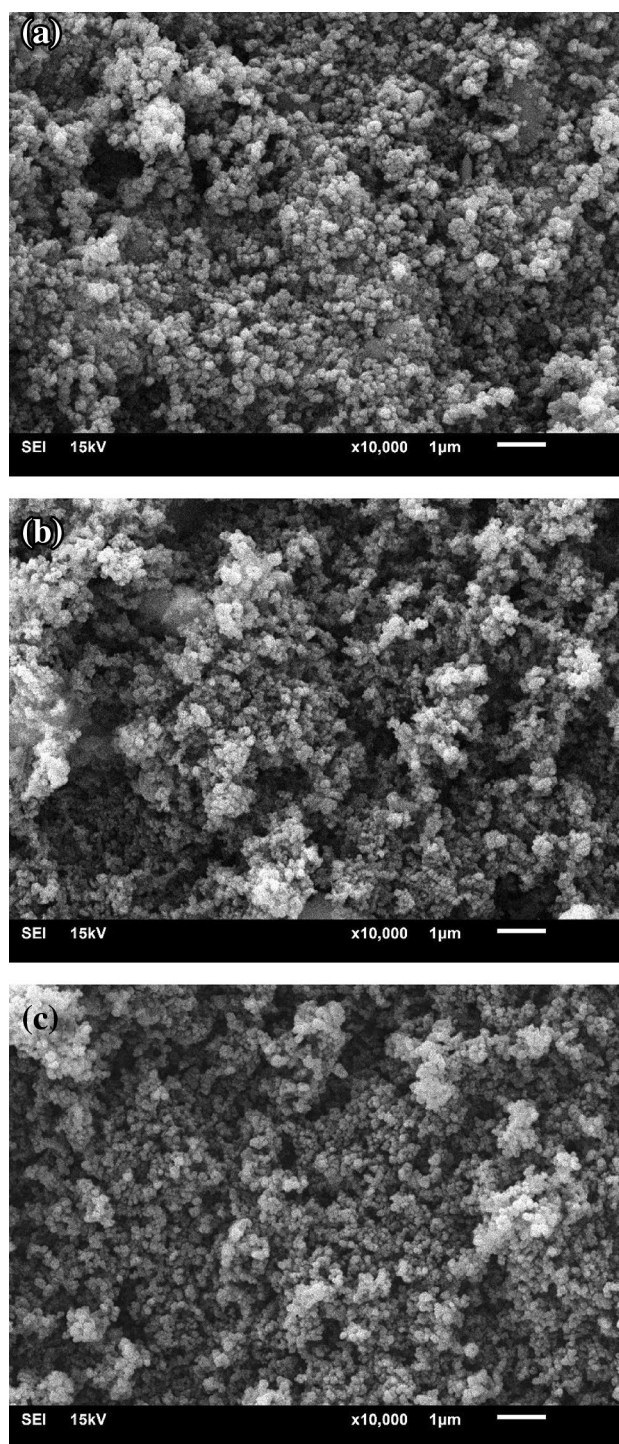


Fig. 3 Presents scanning electron microscopy (SEM) images of three catalysts: **a** Pt/C, **b** PtZr₂/C, and **c** PtZr₂Ni/C

the -0.25 V to 0.1 V CV potential range were attributed to hydrogen adsorption and desorption on the catalyst surface. The electrochemically active surface area of Pt is correlated with the magnitude of these peaks.

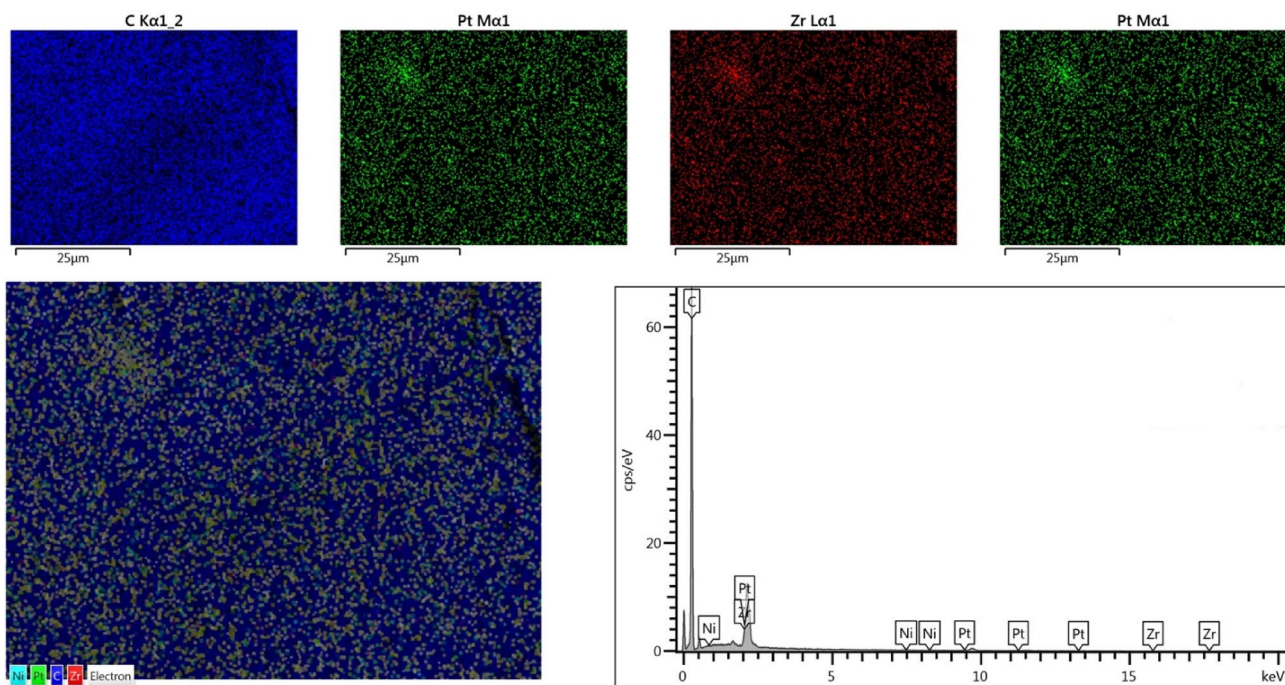


Fig. 4 EDX mapping and analysis for PtZr₂Ni/C catalyst

Table 1 Atomic percent and weight percent of catalysts

	Pt/C		PtZr ₂ /C			PtZr ₂ Ni/C			
	Pt	C	Pt	Zr	C	Pt	Zr	Ni	C
Wt%	18.2	81.8	11.4	6.6	82.0	10.8	6.0	1.2	82.0

The size of the electrochemically active surface area is also critical for increasing oxygen reduction activity [54]. Determining the electrochemically active surface area involves the division of the charge quantities obtained for these peaks by the conversion factor specific to platinum, which is $210 \mu\text{Ccm}^{-2}$ [55–57]. The catalysts Pt/C, PtZr₂/C, and PtZr₂Ni/C have electrochemically active surface areas of 78, 195, and 214 $\text{m}^2\text{g}_{\text{Pt}}^{-1}$, respectively. ECSA increased approximately two and a half times due to the addition of Zr to the Pt/C structure. It was observed that the ECSA value of the PtZr₂Ni/C catalyst formed by adding nickel to the PtZr₂/C structure increased slightly. These values show that PtZr/C and PtZr₂Ni/C catalysts have very high electrochemically active surface areas, but they also indicate that the PtZr/C and PtZr₂Ni/C catalysts have a higher active surface area than the Pt/C catalyst. The large electrochemically active surface area values of PtZr/C and PtZr₂Ni/C were thought to be related to the synergistic effect and the particle sizes. Generally, there is a negative relationship between the size of particles and the electrochemically active surface area (ECSA) value. In other words, catalysts with a large particle size have a

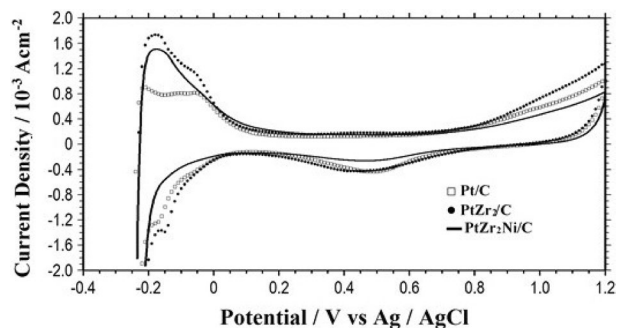


Fig. 5 Cyclic voltammograms of Pt/C, PtZr₂/C, and PtZr₂Ni/C catalysts at a scan rate of 50 mVs^{-1}

low ECSA value, while catalysts with a small particle size have a high ECSA value.

3.2.2 Chronoamperometry and chronopotentiometry measurements

The investigation of stability of catalysts and the electrochemical activity in fuel cells may benefit greatly from

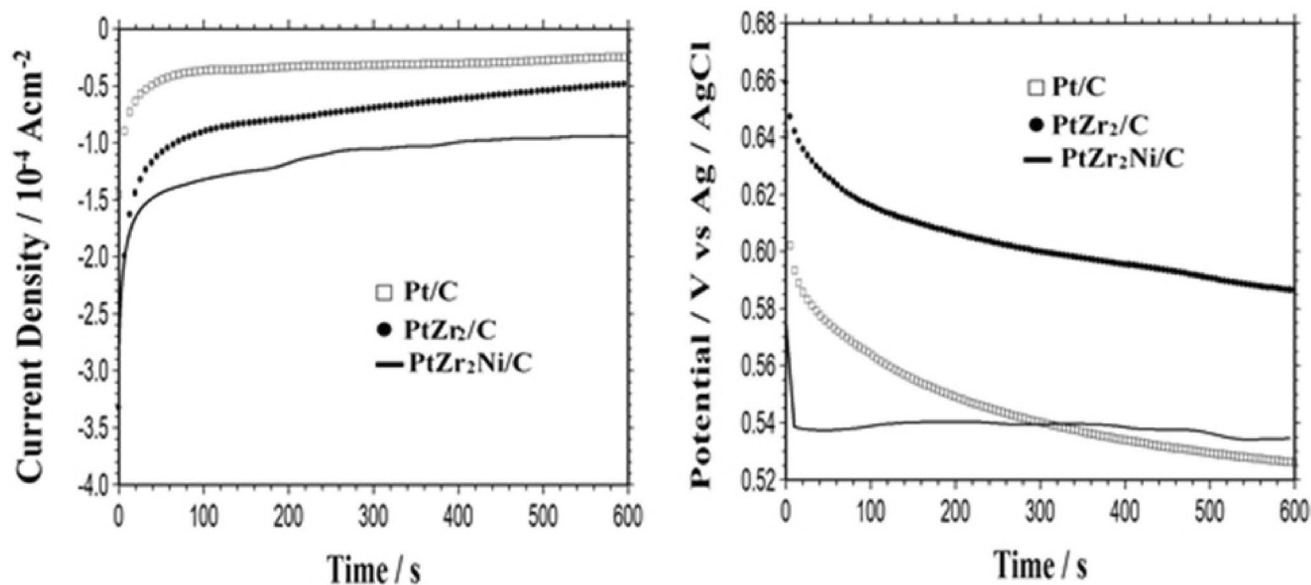


Fig. 6 Chronoamperometry (0.4 V) and chronopotentiometry (2 μ A) curves of the catalysts in 0.5 M H_2SO_4 solution saturated with O_2

chronoamperometric experiments [58, 59]. Chronoamperometry tests on Pt/C, PtZr₂/C and PtZr₂Ni/C catalysts are shown in Fig. 6. It revealed that the change in current values remained remarkably stable after a sharp initial decline. The PtZr₂Ni/C catalyst exhibited superior activity compared to the other catalysts. An increase in electroactivity is indicated by a rise in current density. The current exhibited a rapid decline, despite the fact that the continuous activity reached a stable state at a relatively high current density. Chronopotentiometry is considered a valuable qualitative method for screening catalysts due to its ability to simulate the operation of a fuel cell under a constant current [60]. The potential drop for Pt/C is more significant than that for PtZr/C and PtZr₂Ni/C, as Fig. 6 illustrates based on the starting potential values. Based on these findings, PtZr₂Ni/C is a more potent catalyst than Pt/C and PtZr₂/C.

3.2.3 Electrochemical impedance spectroscopy measurements

For the catalysts Pt/C, PtZr₂/C, and PtZr₂Ni/C, the electrochemical impedance measurements are carried out in O_2 saturated 0.5 M H_2SO_4 solution. Figure 7 shows the Nyquist curves of catalysts. Electrochemical impedance spectroscopy studies of the Nyquist curves in the high-frequency range show a partial semicircle. The charge transfer resistance is represented by the diameter of this incomplete semicircle. The charge transfer resistance increases with increasing diameter. Because the charge transfer resistance and the pace of the electrochemical reaction are inversely correlated, a low charge transfer resistance indicates strong

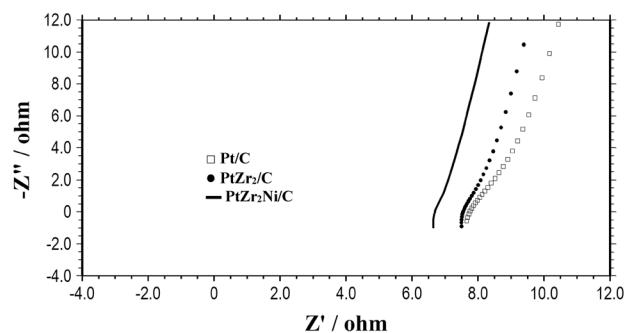


Fig. 7 Nyquist curves of Pt/C, PtZr₂/C, and PtZr₂Ni/C catalysts measured by electrochemical impedance spectroscopy in an O_2 saturated 0.5 M H_2SO_4 solution

electrochemical activity [61]. As can be seen in Fig. 7, the charge transfer resistance of the electrodes with the PtZr₂/C and PtZr₂Ni/C catalysts is lower than that of the electrodes with the Pt/C catalyst because the diameter of the partial semicircles in the high-frequency zone is smaller for the PtZr₂/C and PtZr₂Ni/C catalysts. The value where the Nyquist curves intersect with the X-axis in the high-frequency region shows the equivalent series resistance. Equivalent series resistance includes some resistances such as electrolyte resistance and active material resistance. A lower equivalent series resistance means lower electrical resistance. Equivalent series resistance for the PtZr₂Ni/C is lower than the equivalent series resistance of the PtZr₂/C and Pt/C. These point to greater electrochemical activity in the PtZr₂Ni/C catalyst compared to the Pt/C and PtZr₂/C

catalysts, supporting earlier findings. Chronoamperometry and cyclic voltammetry findings support this theory as well. The observed phenomenon can potentially be elucidated by considering the hypothesis that the electrochemical kinetics of the oxygen reduction reaction (ORR) are enhanced as a result of the increasing current density within the region of low polarization [62].

3.3 Fuel cells performance

The unit cell test served as the final evaluation criterion for the optimal synthesized electrocatalyst. We used electrocatalysts (PtZr/C, PtZr₂/C, and PtZr₃/C) designed for ORR at the cathode for PEM fuel cell testing for the MEA. The Pt/C catalyst served as the anode electrocatalyst for all MEAs. Before sandwich pressing the MEA, the anode and cathode catalysts were evenly brushed onto the GDLs on each side of the Nafion membrane. To maintain the moisture content of the Nafion membrane, the H₂/O₂ gases were subjected to the process of humidification. The electrochemical reactions occur at the interface between the electrolyte and the membrane, specifically on the surface of the catalyst. Hydrogen, fed from one side of the membrane, breaks down into its main components, which are protons and electrons. One electron and one proton make up every hydrogen atom in the universe [63, 64]. Although protons pass through the membrane, electrons pass via external circuits, electrically conducting electrodes, and current collectors, where they perform useful functions before returning to the other side. The protons that have traversed the membrane and the oxygen molecules provided on the same side of the membrane converge at the catalyst sites located at the interface between the membrane and the opposite electrode [65]. The electrochemical reaction produces water, which the cell then expels along with an increased oxygen flow. The concurrent processes result in a continuous flow of electrons along an external circuit, commonly referred to as a direct electrical current. The activation of polarization occurred when the single cell was situated between the open circuit voltage and the higher current density [66, 67].

Figure 8 shows the polarization curves of the cathode electrocatalysts at temperatures ranging from 40 to 70 °C. The efficiency of the single-cell fuel cell diminishes with increasing cell temperature when PtZr/C (1:1), PtZr/C (1:2), and Pt/C catalysts are used as cathode catalysts. The fuel cell efficiency increases as the temperature of the cell increases when PtZr/C (1:3) and PtZr₂Ni/C catalysts are used as the cathode electrocatalysts. The catalysts' active surface area increases as the temperature rises because more activated molecules are present on the surface. Although the Pt:Zr ratios in the PtZr/C electrocatalyst are different, this experiment shows that they significantly affect the performance of the cell not only in the activation region at high voltage

but also during the ohmic field at medium and low voltage. Figure 8e displays the polarization curve of the synthesized PtZr₂Ni/C electrocatalyst upon the addition of Ni to the PtZr₂/C catalyst. The PtZr₂Ni/C electrocatalyst exhibited superior activity compared to the PtZr₂/C electrocatalyst, even at low temperatures. The activity of the PtZr₂Ni/C electrocatalyst's surface area increases with higher cell temperatures. Additionally, when the number of surface cracks decreases, the surface becomes more active. SEM images also confirm this. With increasing cell operating temperatures, the PtZr₂Ni/C electrocatalyst demonstrated better activity than the other catalysts (Fig. 8f). Electrochemical measurements confirmed that the PtZr₂Ni/C electrocatalyst had better performance and surface area than other electrocatalysts.

In the subsequent phase of the study, an ozone-generating generator fed ozone gas to the cathode part in place of oxygen gas. As shown in Fig. 9, adding O₃ gas to the cathode side decreased resistance as the cell temperature in the ohmic loss region decreased compared to using O₂ gas [36, 68].

A pair of coaxial cylindrical electrodes, positioned facing each other, form the generator. A high voltage potential across the electrodes creates a potent electric field that dynamically interacts with the oxygen flow. The aforementioned phenomenon leads to the generation of oxygen radicals. The hydrogen/ozone PEMFCs recorded an observed open circuit voltage (OCV) of 1.65 V, which is significantly higher than the OCV of the hydrogen/oxygen PEMFCs [35, 69, 70]. At a point that is referred to as “the attained current density” [36, 41, 71], there is a sudden voltage drop, and the cell starts to act like that of an H₂/O₂ PEMFC when the current density is 10 mAcm⁻². The increase in power density causes an elevation in the H₂/O₃ PEMFC polarization curve, surpassing the H₂/O₂ PEMFC polarization curve. As the fuel cell temperature rose, the performance of hydrogen–oxygen (H₂/O₂) and hydrogen–ozone (H₂/O₃) PEMFCs went down as the fuel cell temperature went up. This phenomenon was particularly evident when we used PtZr/C and PtZr₂/C catalysts as the cathode electrocatalysts. However, it was observed that the performance of the PtZr₃/C and PtZr₂Ni/C catalysts demonstrated an improvement with the elevation of temperature. The polarization curves of Pt/C, PtZr₂/C, and PtZr₂Ni/C electrocatalysts used as cathode catalysts revealed that the activity of PtZr₂Ni/C electrocatalyst outperformed other electrocatalysts at the 70 °C cell temperature of H₂/O₃ PEM fuel cells (Fig. 9f). Table 2 displays the voltage–current density and power density of the electrocatalysts used in PEMFCs operating at various temperatures.

At 70 °C cell operating temperature, the performance of PEMFCs using H₂/O₂ was 165.87 mWcm⁻² with the maximum power density obtained by the PtZr₂Ni/C cathode catalyst, while maximum power densities of 64.68 mWcm⁻²,

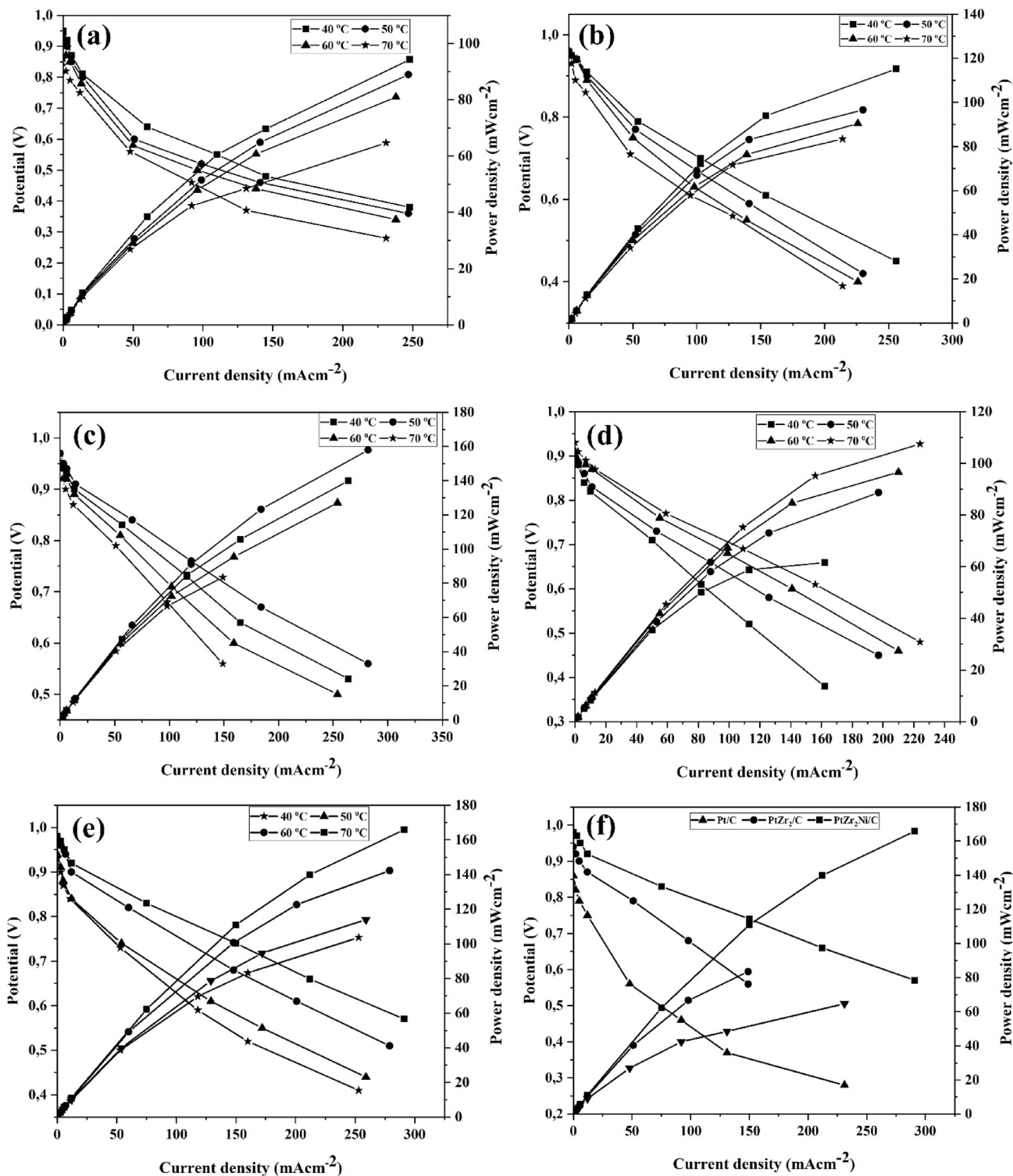


Fig. 8 Polarization curves for **a** Pt/C ($0.15 \text{ mg(Pt)cm}^{-2}$), **b** PtZr/C ($0.13 \text{ mg(Pt)cm}^{-2}$), **c** PtZr₂/C ($0.10 \text{ mg(Pt)cm}^{-2}$), **d** PtZr₃/C ($0.075 \text{ mg(Pt)cm}^{-2}$), **e** PtZr₂Ni/C ($0.035 \text{ mg(Pt)cm}^{-2}$), and **f** 70 °C cell temperature

83.46 mWcm^{-2} , 83.44 mWcm^{-2} , and 107.52 mWcm^{-2} were achieved for the Pt/C, PtZr/C, PtZr₂/C, and PtZr₃/C cathode catalysts, respectively. At the same temperature, using

H₂/O₃, the maximum power density obtained by PtZr₂Ni/C cathode catalyst was 242.08 mWcm^{-2} , while the maximum power densities of Pt/C, PtZr/C, PtZr₂/C, and PtZr₃/C

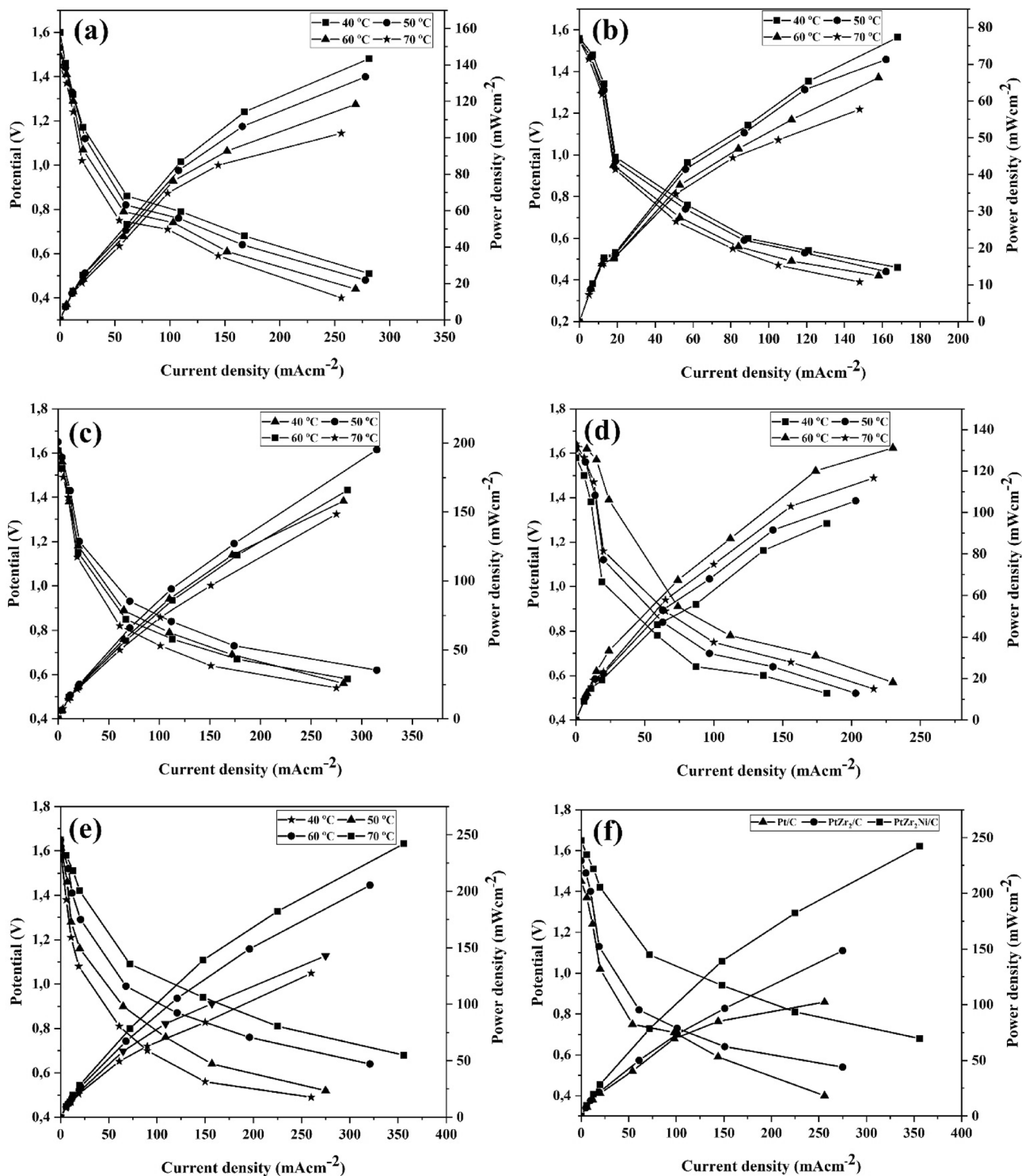


Fig. 9 Polarization curves of **a** Pt/C, **b** PtZr/C, **c** PtZr₂/C, **d** PtZr₃/C, **e** PtZr₂Ni/C, and **f** comparison of Pt/C, PtZr₂/C, and PtZr₂Ni/C catalysts at 70 °C cell temperature

cathode catalysts were 102.40 mWcm⁻², 57.72 mWcm⁻², 148.5 mWcm⁻² and 116.64 mWcm⁻², respectively. For the PtZr₂Ni/C catalyst in the use of H₂/O₂ and H₂/O₃, the peak power has been reported to be 165.87 mWcm⁻² and

242.08 mWcm⁻², which is much higher than the power recorded in cells with Pt and various Pt:Zr atomic compositions, which is noteworthy, respectively.

Table 2 Performance of catalysts in H₂/O₂ and H₂/O₃

Tem.(°C)	H ₂ /O ₂				H ₂ /O ₃			
	OCV (V)	Operating voltage (V)	Current density (mWcm ⁻²)	Power density (mWcm ⁻²)	OCV (V)	Operating voltage (V)	Current density (mAcm ⁻²)	Power density (mWcm ⁻²)
Pt/C								
40	0.95	0.38	248	94.24	1.60	0.51	281	143.31
50	0.94	0.36	247	88.92	1.53	0.48	278	133.44
60	0.90	0.34	238	80.92	1.49	0.44	269	118.36
70	0.86	0.37	231	64.68	1.45	0.40	256	102.40
PtZr/C								
40	0.96	0.45	256	115.2	1.56	0.46	168	77.28
50	0.96	0.42	230	96.60	1.55	0.44	162	71.28
60	0.96	0.40	226	90.40	1.55	0.42	158	66.36
70	0.95	0.39	214	83.46	1.55	0.39	148	57.72
PtZr₂/C								
40	0.97	0.53	264	139.92	1.61	0.56	282	157.92
50	0.97	0.56	282	157.92	1.65	0.62	315	195.30
60	0.95	0.50	254	127.00	1.61	0.58	286	165.98
70	0.94	0.56	149	83.44	1.55	0.54	275	148.50
PtZr₃/C								
40	0.9	0.38	162	61.56	1.58	0.52	182	94.64
50	0.9	0.45	197	88.65	1.62	0.52	203	105.56
60	0.91	0.46	210	96.60	1.64	0.57	230	131.10
70	0.93	0.48	224	107.52	1.64	0.54	216	116.64
PtZr₂Ni/C								
40	0.93	0.41	253	103.73	1.61	0.49	260	127.40
50	0.93	0.44	259	113.96	1.63	0.52	275	143.00
60	0.98	0.51	279	142.29	1.65	0.64	321	205.44
70	0.98	0.57	291	165.87	1.65	0.68	356	242.08

Single-cell polarization data show that Pt-painted spinal has improved fuel cell performance by encouraging the ORR process. The ORR catalytic activity of the synthesized electrocatalysts was found to be PtZr₂Ni/C > PtZr₂/C > PtZr/C > Pt/C > PtZr₃/C when using H₂/O₂, but it was PtZr₂Ni/C > PtZr₂/C > Pt/C > PtZr₃/C > PtZr/C when using H₂/O₃.

One could be said that the utilization of ozone instead of oxygen exhibits an enhancement in the efficacy of PtZr₃/C catalysts, which are characterized by suboptimal reactivity. Therefore, it can be stated that the following factors contribute to the performance decline with rising temperatures: (1) The act of monitoring the voltage of the cell and ascertaining resistances associated with ohmic, charge transfer, and diffusion phenomena during ozone exposure provides evidence that the injection of ozone substantially accelerates the degradation rate of the MEA [42, 43]. Following the introduction of ozone into the system, it was observed that the measurements of the catalyst's surface area change would result in a decrease in the catalyst's activity [42, 44]. (2) The presence of ozone has been observed to hinder the

rates at which protons and water are transferred in the process of oxygen reduction. However, it has also been found to accelerate the dissolution of platinum (Pt) particles in the catalyst [42, 45, 72, 73] and Additionally, the inclusion of cationic species such as Zr metal in the membrane leads to an increase in resistance [31, 54, 56, 57]. As a result, when the Pt:Ni atomic ratio is low (high Zr content is present), a low degree of catalyst aggregation with a high level of dispersion is seen. A tiny number of pores are formed on the electrode layer as a consequence of this.

Consequently, less fuel is transferred from the electrode layer to the cathode, resulting in a higher OCV. The values of the potential and the current density may be utilized to show the oxygen reduction reaction activity of the dual electrocatalyst while taking into account the impact of the Pt:Zr atomic ratios on the performance of the cell in the activation-controlled area [74]. The PtZr/C electrocatalyst's ORR activity increases as Zr concentration in the catalyst increases. This suggests that the Zr content of the PtZr/C electrocatalyst greatly affected ORR activity. Likewise, it

was observed that doping Ni metal to the PtZr₂/C catalyst further increased the activity of the electrocatalyst.

4 Conclusion

In this study, Pt/C, PtZr_x/C ($x = 1, 2, 3$), and PtZr₂Ni/C electrocatalysts were produced for ORR and PEM fuel cells. The studies, conducted at four different temperatures, determined that the PtZr₂Ni/C catalyst was the most active electrocatalyst as a cathode. The face-centered cubic structure of Pt was found to be compatible with the diffraction peaks seen in Pt/C, PtZr₂/C, and PtZr₂Ni/C catalysts. As the electrochemical experiment showed, the PtZr₂/C catalyst had a higher peak current density and more electrocatalytic activity than the Pt/C catalyst, but it had a lower starting potential. The presence of Zr resulted in a decrease in particle size while increasing ECSA. Electrochemical measurements and physical analysis determined that the PtZr₂Ni/C catalyst was more active than the PtZr₂/C catalyst, and high temperature PEM fuel cell applications detected it. Likewise, the presence of Ni metal reduced the particle size and made the catalyst surface more active than Zr metal. In the performance of the PEM fuel cell, the PtZr₂Ni/C catalyst showed good activity not only in the activation loss region but also in the ohmic and concentration loss regions, compared to both Pt/C and at different atomic ratios Pt:Zr catalysts. The PtZr₂Ni/C cathode electrocatalyst's performance increased as the cell temperature rose. Additionally, both H₂/O₂ and H₂/O₃ demonstrated strong performance in both applications, yielding maximum power densities of 165.87 mWcm⁻² and 242.8 mWcm⁻², respectively. The PtZr₂Ni/C electrocatalyst achieved the highest ORR activity and peak power. The ORR catalytic activity of the cathode electrocatalysts was found to be PtZr₂Ni > PtZr₂/C > PtZr/C > Pt/C > PtZr₃/C when using H₂/O₂, but it was PtZr₂Ni > PtZr₂/C > Pt/C > PtZr₃/C > PtZr/C when using H₂/O₃. The higher performance of the PtZr₂Ni/C catalyst is assumed to be a result of its uniformly dispersed nanoparticles and more crystalline lattice defects. The findings show that the PtZr₂Ni/C catalyst had great activity, which had a big effect on the performance of the PEM fuel cell and the activity of the cathode electrocatalyst. Since the PtZr₂Ni/C catalysts described in this article have excellent characteristics and are simple to fabricate, it is anticipated that future studies will result in less expensive electrocatalysts for PEM fuel cells that are currently being developed.

Acknowledgements The authors would like to express their gratitude to the Research Foundation of Siirt University for providing financial assistance via project 2021- SIÜSBF-10.

Author contributions Credit Authorship Contribution Statement AE: Project administration, Writing - original draft. ÖŞ: Project administration- review & editing. AA: Electrochemical measurements and comments SH: Interpretations of physical measurements

Declarations

Conflict of interest The authors declare no competing interests.

References

1. Wang Y, Wang X, Wang X, Liu T, Zhu T, Liu S et al (2021) Droplet dynamic characteristics on PEM fuel cell cathode gas diffusion layer with gradient pore size distribution. *Renew Energy* 178:864–874
2. Çögenli M, Mukerjee S, Yurtcan AB (2015) Membrane electrode assembly with ultra low platinum loading for cathode electrode of PEM fuel cell by using sputter deposition. *Fuel Cells* 15(2):288–297
3. Huo S, Shi W, Wang R, Lu B, Wang Y, Jiao K et al (2021) Elucidating the operating behavior of PEM fuel cell with nickel foam as cathode flow field. *Sci China Technol Sci* 64(5):1041–1056
4. Litster S, McLean G (2004) PEM fuel cell electrodes. *J Power Sources* 130(1–2):61–76
5. Şahin Ö, Akdağ A, Horoz S, Ekinçi A (2023) Physical and electrochemical effect of bimetallic Pd–Mo nanoalloys supported on Vulcan XC-72R carbon as cathode catalysts for proton exchange membrane fuel cell. *Electrocatalysis* 14:202–212
6. Xia L, Tao S, Ni M, Wang Y, Wu C, Xu Q et al (2022) Reconstruction and optimization of catalyst layer of high temperature proton exchange membrane fuel cell. *Int J Hydrogen Energy* 47(84):35778–35789
7. Zhao X, Sasaki K (2022) Advanced Pt-based core–shell electrocatalysts for fuel cell cathodes. *Acc Chem Res* 55(9):1226–1236
8. Sammes N (2006) *Fuel cell technology: reaching towards commercialization*. Springer Science & Business Media, Cham
9. Rahsepar M, Pakshir M, Piao Y, Kim H (2012) Preparation of highly active 40 wt.% Pt on multiwalled carbon nanotube by improved impregnation method for fuel cell applications. *Fuel Cells* 12(5):827–834
10. Yang H, Lee W, Choi B, Ko Y, Yi S, Kim W (2017) Self-humidifying Pt-C/Pt-TiO₂ dual-catalyst electrode membrane assembly for proton-exchange membrane fuel cells. *Energy* 120:12–19
11. Fofana D, Natarajan SK, Hamelin J, Benard P (2014) Low platinum, high limiting current density of the PEMFC (proton exchange membrane fuel cell) based on multilayer cathode catalyst approach. *Energy* 64:398–403
12. Sahoo M, Ramaprabhu S (2017) Nitrogen and sulfur co-doped porous carbon—is an efficient electrocatalyst as platinum or a hoax for oxygen reduction reaction in acidic environment PEM fuel cell? *Energy* 119:1075–1083
13. Fan L, Zhao J, Luo X, Tu Z (2022) Comparison of the performance and degradation mechanism of PEMFC with Pt/C and Pt black catalyst. *Int J Hydrogen Energy* 47(8):5418–5428
14. Pavlets A, Alekseenko A, Kozhokar E, Pankov I, Alekseenko D, Guterman V (2023) Efficient Pt-based nanostructured electrocatalysts for fuel cells: one-pot preparation, gradient structure, effect of alloying, electrochemical performance. *Int J Hydrogen Energy* 48:22379–22388
15. Chaisuban N, Maniwan W, Hunsom M (2017) Effect of heat-treatment on the performance of PtM/C (M= Cr, Pd, Co) catalysts towards the oxygen reduction reaction in PEM fuel cell. *Energy* 127:454–461
16. Wan X, Liu X, Li Y, Yu R, Zheng L, Yan W et al (2019) Fe–N–C electrocatalyst with dense active sites and efficient mass transport for high-performance proton exchange membrane fuel cells. *Nat Catal* 2(3):259–268
17. Baroutaji A, Carton J, Oladoye A, Stokes J, Twomey B, Olabi A (2017) Ex-situ evaluation of PTFE coated metals in a proton

- exchange membrane fuel cell environment. *Surf Coat Technol* 323:10–17
18. Şahin Ö, Yılmaz A, Ekinçi A (2023) Effect of microwave irradiation on PEMFCs anode and cathode catalysts. *J Aust Ceram Soc* 59:895–904
 19. Ouyang M, Feng Y, Zhang S, Zhang H, Zhu L, Liu S et al (2023) Platinum-nickel bimetallic catalyst doped with rare earth for enhancing methanol electrocatalytic oxidation reaction. *Int J Hydrogen Energy* 48:29518–29529
 20. Çetin SK, Akça G, Kaya D, Ayaş AO, Ekicibil A (2022) Synthesis and characterization of bifunctional Ru doped La-based perovskites for magnetic refrigeration and energy storage systems. *Int J Hydrogen Energy* 47(97):40999–41009
 21. Chang Y-F, Wu C-Y, Chang M-H (2024) Fabrication of platinum-cobalt nanowires by centrifugal electrospinning as oxygen reduction catalyst for PEMFC. *Int J Hydrogen Energy* 54:437–445
 22. Şahin Ö, Akdag A, Horoz S, Ekinçi A (2023) Synthesized PdNi/C and PdNiZr/C catalysts for single cell PEM fuel cell cathode catalysts application. *Fuel* 346:128391
 23. Jang I, Ahn M, Lee S, Yoo SJ (2022) Surfactant assisted geometric barriers on PtNi@C electrocatalyst for phosphoric acid fuel cells. *J Ind Eng Chem* 110:198–205
 24. Kumar PR, Suryawanshi PL, Gumfekar SP, Bhanvase BA, Sonawane S (2018) Sonochemical synthesis of Pt-Co/C electrocatalyst for PEM fuel cell applications. *Surf Interfaces* 12:116–123
 25. Polagani RK, Suryawanshi PL, Gumfekar SP, Sonawane SH, Ashokkumar M (2018) Ultrasound-assisted synthesis of Pt-Co/C bimetallic alloys for oxygen reduction in PEM fuel cells. *Sustain Energy Fuels* 2(7):1491–1499
 26. Polagani RK, Suryawanshi PL, Sonawane SH, Chinthala M (2022) Electrocatalytic performance of sonochemically synthesized Pt-Ni/C nanoparticles in fuel cell application. *Int J Chem React Eng* 20(8):873–885
 27. Polagani RK, Chinthala M, Sonawane SH (2022) The effect of Cr alloying with Pt/C as an electrocatalyst for low temperature PEM fuel cell. *Energy Sources A: Recover Util Environ Eff* 44(2):3239–3252
 28. Bezerra CW, Zhang L, Liu H, Lee K, Marques AL, Marques EP et al (2007) A review of heat-treatment effects on activity and stability of PEM fuel cell catalysts for oxygen reduction reaction. *J Power Sources* 173(2):891–908
 29. Yamazaki S-i, Asahi M, Taguchi N, Ioroi T (2022) Sulphonated melamine polymer for enhancing the oxygen reduction reaction activity and stability of a Pt catalyst. *J Electroanal Chem* 908:116103
 30. Şahin Ö, Yılmaz A, Ekinçi A (2023) Microwave application as an alternative method to increase the efficiency of PtC catalyst in PEMFCs. *Proc Inst Mech Eng A: J Power Energy* 237:1329–1336
 31. Souza IC, Manfro RL, Souza MM (2022) Hydrogen production from steam reforming of acetic acid over Pt–Ni bimetallic catalysts supported on ZrO₂. *Biomass Bioenerg* 156:106317
 32. Liu Y, Ishihara A, Mitsushima S, Kamiya N, Ota K-i (2005) Zirconium oxide for PEFC cathodes. *Electrochem Solid-State Lett* 8(8):A400
 33. Sahu A, Mondal K, Pala RG (2020) Activated porous highly enriched platinum and palladium electrocatalysts from dealloyed noncrystalline alloys for enhanced hydrogen evolution. *ChemElectroChem* 7(21):4405–4416
 34. He G, Zhang R, Zhao Q, Yang S, Jin H, Guo X (2018) Effect of the Cr₂O₃ promoter on Pt/WO₃-ZrO₂ catalysts for n-heptane isomerization. *Catalysts* 8(11):522
 35. Bussayajarn N, Therdtianwong S, Therdtianwong A (2007) Improvement of cathodic reaction of proton exchange membrane fuel cell by ozone. *Int J Hydrogen Energy* 32(3):392–399
 36. Shabani B, Hafttananian M, Khamani S, Ramiar A, Ranjbar A (2019) Poisoning of proton exchange membrane fuel cells by contaminants and impurities: review of mechanisms, effects, and mitigation strategies. *J Power Sources* 427:21–48
 37. Jian J, Hashemi H, Wu H, Jasper AW, Glarborg P (2022) A reaction mechanism for ozone dissociation and reaction with hydrogen at elevated temperature. *Fuel* 322:124138
 38. Von Gunten U (2003) Ozonation of drinking water: part I. Oxidation kinetics and product formation. *Water Res* 37(7):1443–1467
 39. Liu Z, Demeestere K, Van Hulle S (2021) Comparison and performance assessment of ozone-based AOPs in view of trace organic contaminants abatement in water and wastewater: a review. *J Environ Chem Eng* 9(4):105599
 40. Dahake A, Kumar DS, Singh AV (2022) Using ozone and hydrogen peroxide for improving the velocity deficits of gaseous detonations. *Trans Indian Natl Acad Eng* 7(3):1033–1042
 41. Şahin Ö, Akdag A, Horoz S, Ekinçi A (2023) Effects of H₂/O₂ and H₂/O₃ gases on PtMo/C cathode PEMFCs performance operating at different temperatures. *Int J Hydrogen Energy* 48(44):16829–16840
 42. Lovato ME, Martín CA, Cassano AE (2009) A reaction kinetic model for ozone decomposition in aqueous media valid for neutral and acidic pH. *Chem Eng J* 146(3):486–497
 43. Zeng Y, Chen D, Chen T, Cai M, Zhang Q, Xie Z et al (2019) Study on heterogeneous photocatalytic ozonation degradation of ciprofloxacin by TiO₂/carbon dots: kinetic, mechanism and pathway investigation. *Chemosphere* 227:198–206
 44. John A, Brookes A, Carra I, Jefferson B, Jarvis P (2022) Microbubbles and their application to ozonation in water treatment: a critical review exploring their benefit and future application. *Crit Rev Environ Sci Technol* 52(9):1561–1603
 45. Gao D, Cai F, Xu Q, Wang G, Pan X, Bao X (2014) Gas-phase electrocatalytic reduction of carbon dioxide using electrolytic cell based on phosphoric acid-doped polybenzimidazole membrane. *J Energy Chem* 23(6):694–700
 46. Fan Q, Yu H, Wang T-G, Wu Z, Liu Y (2017) Preparation and isothermal oxidation behavior of zr-doped, pt-modified aluminide coating prepared by a hybrid process. *Coatings* 8(1):1
 47. Zhang H, Zeng Y, Cao L, Yang L, Fang D, Yi B et al (2017) Enhanced electrocatalytic performance of ultrathin PtNi alloy nanowires for oxygen reduction reaction. *Front Energy* 11:260–267
 48. Behmenyar G, Akın AN (2014) Investigation of carbon supported Pd–Cu nanoparticles as anode catalysts for direct borohydride fuel cell. *J Power Sources* 249:239–246
 49. Yi L, Wei W, Zhao C, Yang C, Tian L, Liu J et al (2015) Electrochemical oxidation of sodium borohydride on carbon supported Pt-Zn nanoparticle bimetallic catalyst and its implications to direct borohydride-hydrogen peroxide fuel cell. *Electrochim Acta* 158:209–218
 50. Do CL, San Pham T, Nguyen NP, Tran VQ, Pham HH (2015) Synthesis and characterization of alloy catalyst nanoparticles PtNi/C for oxygen reduction reaction in proton exchange membrane fuel cell. *Adv Nat Sci: Nanosci Nanotechnol* 6(2):025009
 51. Liu J, Yi L, Wang X, Zhao Q, Zhang Y, Gao J et al (2015) Investigation of nanoporous carbon supported palladium–zinc nanocomposites as anode catalysts for direct borohydride–hydrogen peroxide fuel cell. *Int J Hydrogen Energy* 40(23):7301–7307
 52. Wang Z, Yin G, Shi P, Sun Y (2005) Novel Pt–Ru–Ni/C catalysts for methanol electro-oxidation in acid medium. *Electrochem Solid-State Lett* 9(1):A13
 53. da Silva FT, Dalmazzo VA, Becker MR, de Souza MO, de Souza RF, Martini EM (2014) Effect of Ni proportion on the performance of proton exchange membrane fuel cells using PtNi/C electrocatalysts. *Ionics* 20:381–388

54. Shapovalov SS, Mayorova NA, Modestov AD, Shiryaev AA, Egorov AV, Grinberg VA (2022) Pt-Mo/C, Pt-Fe/C, and Pt-Mo-Sn/C nanocatalysts derived from cluster compounds for proton exchange membrane fuel cells. *Catalysts* 12(3):255
55. Campbell S, Smith J, Lloyd G, Walsh F, Ralph T (1998) Electrochemical and microscopic characterisation of platinum-coated perfluorosulfonic acid (Nafion 117) materials. *Analyst* 123(10):1923–1929
56. Oh H-S, Kim H-S (2010) Noncovalent modification of carbon nanofibers using 2-naphthalenethiol for catalyst supports in PEM fuel cells. *J Electrochem Sci Technol* 1(2):92–96
57. Luo L, Abbo HS, Titinchi SJ, Tsiakaras P, Yin S (2019) Highly efficient electrocatalysts for oxygen reduction reaction: nitrogen-doped PtNiMo ternary alloys. *Int J Hydrogen Energy* 44(13):6582–6591
58. Liu X, Yi L, Wang X, Su J, Song Y, Liu J (2012) Graphene supported platinum nanoparticles as anode electrocatalyst for direct borohydride fuel cell. *Int J Hydrogen Energy* 37(23):17984–17991
59. Eris S, Daşdelen Z, Sen F (2018) Enhanced electrocatalytic activity and stability of monodisperse Pt nanocomposites for direct methanol fuel cells. *J Colloid Interface Sci* 513:767–773
60. Atwan MH, Macdonald CL, Northwood DO, Gyenge EL (2006) Colloidal Au and Au-alloy catalysts for direct borohydride fuel cells: electrocatalysis and fuel cell performance. *J Power Sources* 158(1):36–44
61. Zhang Y, Hu Y, Li S, Sun J, Hou B (2011) Manganese dioxide-coated carbon nanotubes as an improved cathodic catalyst for oxygen reduction in a microbial fuel cell. *J Power Sources* 196(22):9284–9289
62. Xie Z, Holdcroft S (2004) Polarization-dependent mass transport parameters for ORR in perfluorosulfonic acid ionomer membranes: an EIS study using microelectrodes. *J Electroanal Chem* 568:247–260
63. Wang Y, Pang Y, Xu H, Martinez A, Chen KS (2022) PEM Fuel cell and electrolysis cell technologies and hydrogen infrastructure development—a review. *Energy Environ Sci* 15(6):2288–2328
64. Fan L, Tu Z, Chan SH (2023) Recent development in design a state-of-art proton exchange membrane fuel cell from stack to system: theory, integration and prospective. *Int J Hydrogen Energy* 48(21):7828–7865
65. Maier M, Smith K, Dodwell J, Hinds G, Shearing P, Brett D (2022) Mass transport in PEM water electrolyzers: a review. *Int J Hydrogen Energy* 47(1):30–56
66. Mohanraju K, Cindrella L (2014) Impact of alloying and lattice strain on ORR activity of Pt and Pd based ternary alloys with Fe and Co for proton exchange membrane fuel cell applications. *RSC Adv* 4(23):11939–11947
67. Van Der Linden F, Pahon E, Morando S, Bouquain D (2023) A review on the proton-exchange membrane fuel cell break-in physical principles, activation procedures, and characterization methods. *J Power Sources* 575:233168
68. Li C, Wang L, Wang X, Kong M, Zhang Q, Li G (2017) Synthesis of PVDF-g-PSSA proton exchange membrane by ozone-induced graft copolymerization and its application in microbial fuel cells. *J Membr Sci* 527:35–42
69. Jarchlouei MA, Chitsaz A, Mahmoudi S, Rosen MA, Bafekr SH (2021) Gibbs energy minimization using Lagrange method of undetermined multipliers for electrochemical and thermodynamic modeling of a MCFC with internal steam reforming. *Energy Convers Manage* 228:113594
70. Roh G, Lee H, Jeong Y, Kim JH, Kim H (2019) Preparation of carbon-supported Pt–Ru core-shell nanoparticles using carbonized polydopamine and ozone for a CO tolerant electrocatalyst. *Int J Hydrogen Energy* 44(39):21588–21596
71. Franck-Lacaze L, Bonnet C, Besse S, Lapique F (2009) Effects of ozone on the performance of a polymer electrolyte membrane fuel cell. *Fuel Cells* 9(5):562–569
72. Trombetta F, Lima DW, Fiegenbaum F, Becker MR, de Souza MO, Martini EM (2018) C16MI. OTf ionic liquid on Pt/C and PtMo/C anodes improves the PEMFC performance. *Int J Hydrogen Energy* 43(14):6945–6953
73. Vermaak L, Neomagus HW, Bessarabov DG (2021) The CO tolerance of Pt/C and Pt-Ru/C electrocatalysts in a high-temperature electrochemical cell used for hydrogen separation. *Membranes* 11(9):670
74. Camara GA, Giz MJ, Paganin VA, Ticianelli EA (2002) Correlation of electrochemical and physical properties of PtRu alloy electrocatalysts for PEM fuel cells. *J Electroanal Chem* 537(1–2):21–29

Publisher's Note Springer Nature remains neutral with regard to jurisdictional claims in published maps and institutional affiliations.

Springer Nature or its licensor (e.g. a society or other partner) holds exclusive rights to this article under a publishing agreement with the author(s) or other rightsholder(s); author self-archiving of the accepted manuscript version of this article is solely governed by the terms of such publishing agreement and applicable law.

Authors and Affiliations

Abdurrahman Akdag¹ · Sabit Horoz² · Ömer Şahin³ · Arzu Ekinci⁴

✉ Arzu Ekinci
aekinci@siirt.edu.tr

Abdurrahman Akdag
aakdag@harran.edu.tr

Sabit Horoz
sabit.horoz@sivas.edu.tr

Ömer Şahin
omersahin@itu.edu.tr

² Metallurgical and Materials Engineering, Sivas Science and Technology University, Sivas, Turkey

³ Department of Chemical Engineering, Faculty of Chemical and Metallurgical Engineering, Istanbul Technical University, Istanbul, Turkey

⁴ Department of Occupational Health and Safety, Faculty of Health Sciences, Siirt University, Siirt, Turkey

¹ Vocational School of Health Services, Harran University, Sanliurfa, Turkey